

Article

Analysis of the Oxidation Behavior and Formation of an Extremely Thin Oxide Layer with a Novel Hot-Stamped Steel

Yan Zhao ^{1,2} , Lei Liu ^{1,2} , Dengcui Yang ³, Weinan Li ^{1,2}, Jianlin Yu ⁴ and Zhengzhi Zhao ^{1,2,*} 

¹ Collaborative Innovation Center of Steel Technology, University of Science and Technology Beijing, Beijing 100083, China; b20200553@xs.ustb.edu.cn (Y.Z.); g124173@163.com (L.L.); m202221342@xs.ustb.edu.cn (W.L.)

² Beijing Engineering Technology Research Center of Special Steel for Traffic and Energy, Beijing 100083, China

³ Department of Mining Engineering, Shanxi Institute of Energy, Jinzhong 030604, China; yangdc@sxie.edu.cn

⁴ Xinyu Iron and Steel Group Co., Ltd., Xinyu 338001, China; yjl@xinsteel.com.cn

* Correspondence: zhaozhzhi@ustb.edu.cn

Abstract: This study investigates enhancing the high-temperature oxidation resistance of hot-stamped steels by adding the Cr/Mn/Si elements to form an extremely thin oxide layer. Under low oxygen partial pressure conditions and high Cr content in the matrix, the oxide layer of a 38Cr3MnNbVMo hot-rolled plate containing the Mo element and high Si content was further thinned to 0.6 μm after cooling at 900 °C for 5 min. The structure of the ultra-thin oxide layer consists of Fe_3O_4 , Mn oxides, FeCr_2O_4 , Cr_2O_3 , and Fe_2SiO_4 oxides. Compared to other antioxidant elements, under low oxygen partial pressure conditions, Si is more prone to oxidation, forming ultra-thin (22 nm) Fe_2SiO_4 oxides at the matrix interface. Combined with Cr_2O_3 , FeCr_2O_4 , and Mn oxides, it collectively inhibits the mutual diffusion of external O ions and matrix Fe ions. Furthermore, the addition of the Mo element improves the oxidation resistance. The synergistic effect of multiple powerful oxidation-resistant elements and oxide products effectively inhibits the growth of the iron oxide scale, enhancing the oxidation resistance of hot-rolled, hot-stamped steel.

Keywords: 38Cr3MnNbVMo hot-stamped steel; high-temperature oxidation resistance; extremely thin oxide layer; Fe_2SiO_4 and FeCr_2O_4 oxides



Citation: Zhao, Y.; Liu, L.; Yang, D.; Li, W.; Yu, J.; Zhao, Z. Analysis of the Oxidation Behavior and Formation of an Extremely Thin Oxide Layer with a Novel Hot-Stamped Steel. *Metals* **2024**, *14*, 760. <https://doi.org/10.3390/met14070760>

Academic Editor: Rastko Vasilic

Received: 29 May 2024

Revised: 17 June 2024

Accepted: 26 June 2024

Published: 27 June 2024



Copyright: © 2024 by the authors. Licensee MDPI, Basel, Switzerland. This article is an open access article distributed under the terms and conditions of the Creative Commons Attribution (CC BY) license (<https://creativecommons.org/licenses/by/4.0/>).

1. Introduction

The application of the most widely used hot-stamped steel is 22MnB5 in automobiles. As an ultra-high-strength structural material, 22MnB5 hot-stamped steel is used in the structural components of automobile bodies, mainly including Al-Si coating, nano-Zn coating, and a bare plate [1,2]. As the protective layer, a steel plate with Al-Si coating avoids surface oxidation effectively during the hot stamping process. However, it is difficult to weld and reduce the service life of the inner roller; its production cost is too high [3]. The bare hot-stamped sheet shows a low production cost, but the surface of the steel sheet makes it easy to form an oxide layer in the process of heating and hot stamping, and the stamping parts are easy to corrode [3]. In the process of hot stamping, the sheet is fed by a manipulator in the air. At a high temperature, the steel plate oxidizes to a certain extent in contact with the air, and the oxide layer appears on its surface. In the hot stamping process, the oxide layer falls off, which not only affects the beauty and surface quality of the work piece, but also causes certain wear to die [4]. Therefore, the study of high-temperature oxidation behavior of hot-stamped steel is the significant link to improving surface quality.

In order to improve the surface quality of hot-stamped steel, enhancing the oxidation resistance and replacing the Al-Si coating, it is necessary to design a high Cr-Si-Mn alloy composition system to control the oxide layer thickness. Some researchers have adopted Cr-Si alloying and applied it to 22MnB5 hot-stamped steel. The transformation-induced plasticity (TRIP) effect of retained austenite showed the excellent product of strength and

elongation, bending toughness, and hydrogen brittleness resistance [5–8]. Therefore, while ultra-high-strength steel met the good mechanical properties and service performance, Cr and Si were used in hot-stamped steel, resulting in superior antioxidant properties. In ultra-high-strength steel, Si elements formed spinel compounds at the matrix interface and were embedded in the matrix, which increased the binding force between the oxide scale and the matrix. The continuous enrichment of Si at the interface hindered the external oxidation process of Fe ions and weakened the thickness of the oxide scale [9,10]. The effect of Cr was similar to the Si element, and the affinity between Cr and O was much greater than that of Fe. In the process of high-temperature heating, the Cr atom showed higher mobility, and selective oxidation occurred at the interface of the steel sheet, forming a dense oxide layer. The dense oxide layer of the Cr compound played an essential role in improving the oxidation resistance of the matrix [11,12]. In addition, the addition of Mn also represented a positive effect on the high temperature oxidation resistance [12]. Li et al. [13] studied the oxidation resistance of new hot-stamping steel with Cr, Si, and Mn alloying elements. During the hot stamping process, the Si and Mn elements in the new hot-stamping steel promoted the formation of a continuous Cr_2O_3 layer which had a good protective effect, thus improving the high-temperature oxidation resistance of the hot-stamped steel. Hou et al. [14] explored the feasibility and advantages of a new type of non-plated, oxidation-resistant thermoformed steel with rapid heating (over $100\text{ }^\circ\text{C/s}$) to a full austenitizing temperature of $930\text{ }^\circ\text{C}$ for 120 s. The experiment showed that after rapid heating and holding for 120 s under N_2 conditions, the oxide layer thickness of the non-coated hot-formed steel is less than $5\text{ }\mu\text{m}$, which was more than seven times thinner than the oxide layer thickness of 22MnB5 hot-stamped steel ($36\text{ }\mu\text{m}$) under the same process. Compared with the traditional austenitizing process (holding at $930\text{ }^\circ\text{C}$ for 5 min), the rapid heating process shortened the austenitizing time (2 min). It not only saved energy consumption but also significantly reduced the thickness of the oxide layer. Therefore, it led to the elimination of the need for shot peening and further improved the oxidation resistance.

However, concerning the rigorous requirements of energy saving and environmental protection, there is an urgent demand to develop ultra-high-strength steel to meet the dual requirements of automotive lightweight and safety performance. The most effective means is to improve the strength of steel materials. In the previous research, we designed novel hot-stamped steel through composition design, process optimization, and microstructure evolution. The tensile strength was greater than 2100 MPa and the total elongation was greater than 7.0% [15,16]. As we carried out the oxidation experiment, the condition of the high-temperature experiment was air. In order to further promote the oxidation resistance, the high-temperature environment was set to argon.

2. Materials and Methods

The novel hot-rolled, hot-stamped steel was named as 38Cr3MnNbVMo, compared with the hot-rolled 22MnB5 steel. The specific chemical composition is shown in Table 1 [15]. First, the studied steel was cut into a rectangular sample size of $10\text{ mm} \times 6\text{ mm}$ for the observation and analysis of the cross-section morphology of the oxide sheet. The surfaces of all samples were polished with 1000# sandpaper and cleaned and dried with alcohol before oxidation experiment. Oxidation experiments were carried out in a high-temperature tube heat treatment furnace with argon gas and air. The heating temperature was selected at $900\text{ }^\circ\text{C}$ and the soaking time was 5 min. Tubular furnace KSL-1100X was made in China, Hefei Kejing Technology Material Co., Ltd. (Hefei, China). The oxidized sample was cold-mounted and polished with epoxy resin, using 4% nitrate alcohol to erode the oxide layer so that the oxide layer had a certain layered structure. The back-scattering diffraction (BSD) mode was used to observe the oxide layer formed at a high temperature of hot-rolled, hot-stamped steel with a voltage of 20 kV and a working distance of $10\text{ mm}\sim 12\text{ mm}$. The element distribution of the oxide layer was analyzed by means of Scanning Electron Microscope Energy Dispersive Spectrometer (SEM-EDS) and Electron

Probe Micro Analyzer (EPMA). Sigma500 field emission scanning electron microscope was developed by Germany Zeiss company (Oberkochen, Germany). EPMA-1720H was developed by Shimadzu Corporation of Japan (Kyoto, Japan). The oxidized samples were stored in a vacuum bag, the oxide layer TEM samples were prepared by focused ion beam (FIB), and the transmission experiments were carried out by JEM-2100 transmission electron microscopy. JEM-2100 transmission electron microscopy was made at the Japan JEOL Company (Tokyo, Japan). Focused ion beam (FIB) was made in the United States, FEI HELIOS G4 UC Company (Hillsboro, OR, USA). The phase of oxidation layer was analyzed by X-ray diffraction and the oxidation resistance of ultra-high-strength hot-stamped steel was evaluated. The diffraction angle range of the oxide layer was $10^\circ/20^\circ\sim 90^\circ$, and the step size was 0.2° . X-ray diffraction was made in Mannheim, Germany, Bruker company.

Table 1. The composition of hot-stamped steels (wt.%).

Steel Grade	C	Si	Mn	Cr	Nb + V	Mo	Ti/B
38Cr3MnNbVMo	0.35~0.42	1.10~1.60	1.10~1.60	2.0~3.0	≤ 0.25	0.10~0.30	-
22MnB5	0.22~0.25	0.20~0.30	1.20~1.40	0.15~0.25	-	-	0.025~0.040/0.002~0.004

3. Results and Discussion

Figure 1a,b₁–b₅ illustrates the morphology oxide layer and map-scanning distribution of SEM-EDS, respectively. The oxidation layers of 38Cr3MnNbVMo tested steels are mainly composed of O, Fe, Cr, Mn, and Si elements. The oxidation layer of 38Cr3MnNbVMo steel forms a Cr/Si/Mn enrichment region, which indicates that the formation of Cr/Mn/Si oxidation products further prevents the oxidation of substructure iron. The content of Cr at the interface between the substructure and oxide layer is significantly increased, which is obviously higher than that of the substructure and the outer oxide layer. In addition, the enrichment degree of Si and Mn is less than the Cr element, and the oxide thickness ratio of Cr, Si, and Mn almost covers the entire oxide layer. Figure 1c shows the XRD pattern of the oxide layer of the 38Mn3CrNbVMo studied steel. Due to the thin oxide layer, the prominent peak value is mainly the Fe substructure of the BCC structure, and several shorter peaks portray Fe₃O₄ and Fe₂O₃; the most significant are spinel FeCr₂O₄ and olivine Fe₂SiO₄. Combined with Figure 1d,e, Table 2 shows the element mass fraction of SEM-EDS scanning distribution at different positions of the tested steel oxide layers in the image. There is an obvious step difference in Cr content between the interface and the outer oxide layer, while there is a tiny difference in Si and Mn content. The gradient of the Mo element also demonstrated that the Mo element promotes the growth of the oxide layer of Cr, Si, and Mn alloys and forms a dense protective film on the surface of the substructure.

Similarly, the element distribution mapping of the oxide layer of 22MnB5 hot-rolled steel is also characterized by SEM-EDS, as shown in Figure 2. The oxide layer of 22MnB5 is mainly composed of O, Fe, and Si elements, and they are enriched in the secondary oxide layer, while the distribution of other alloying elements is not obvious. The average thickness of the oxide layer is 3.8 μm , but the cross-section in contact with the substrate is spalling, which may be due to the incorporation of some Cr (Cr, Mn)₂O₃ oxides entering into the Fe-rich oxide core shell, leading to the separation oxidation due to extraneous nucleation [17]. That is, the initial chromium-rich oxides do not prevent iron from outwardly diffusing to form iron-rich oxides. Therefore, Figure 2b₁–b₅ shows that only a trace of Si enrichment is formed at the bottom of the oxide layer, and no obvious segregation of Cr/Mn appears at the enrichment region of the secondary oxide layer. Also, it is related to the low content of Cr and Si in 22MnB5. The XRD pattern and EDS line analysis in Figure 2c,d also indicate that Cr elements play a small hindrance role at the interface. Therefore, at the same heating temperature, isothermal time and atmosphere conditions, the oxidation resistance of 22MnB5 steel is not as good as the novel 38Cr3MnNbVMo steel.

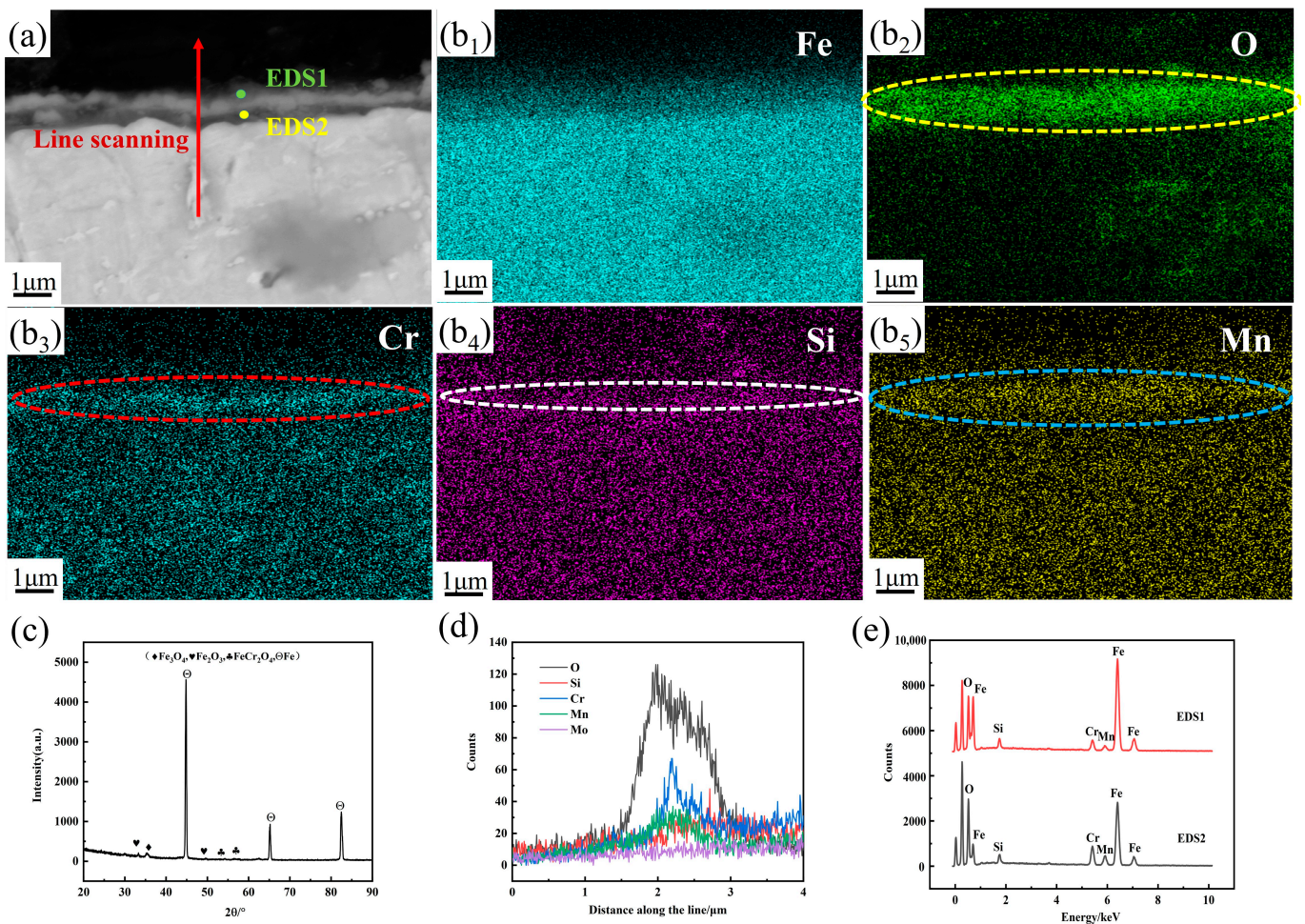


Figure 1. Longitudinal section SEM images of 38Cr3MnNbVMo studied steel soaked at 900 °C for 5 min. (a) The longitudinal section morphology; (b₁–b₅) EDS mapping of oxide region; (c) XRD pattern of oxide layer; (d) EDS line scanning of (a) red arrow; (e) the energy spectrum of different positions.

Table 2. The tested steel oxidized at 900 °C for 5 min at different positions of oxidation layer element mass fraction (wt.%).

Studied Steel	Position	O	Fe	Mn	Cr	Si	Mo
38Cr3MnNbVMo	EDS1	28.0	59.6	5.8	4.3	2.1	0.2
	EDS2	23.6	57.4	5.7	10.2	2.6	0.5

In order to analyze and characterize the ultra-thin oxide layer more accurately and precisely, with the help of EPMA, the element distribution of the 38Cr3MnNbVMo studied steel oxide layer longitudinal section is analyzed and characterized more accurately. Figure 3 shows the EPMA image of oxide layer of 38Cr3MnNbVMo hot-rolled tested steel is held at 900 °C for 5 min at the condition of low oxygen partial pressure. The enrichment of O, Fe, Cr, Mn, and Si elements appears in the oxide layer of the hot-rolled tested steel after the oxidation at low oxygen partial pressure and high temperature.

In accordance with the SEM-EDS results, the enrichment ratio of Cr and Mn is larger in 38Cr3MnNbVMo steel, but the enrichment ratio of Si is smaller. Geneve et al. [18] believed that if the number of Si atoms accumulated in the oxide layer was increasing, then the accumulation of Si atoms depended not only on the composition of the alloy but also on the oxidation conditions. The oxidation experiment reduced the partial pressure of oxygen and facilitated the formation of stable oxides, such as SiO₂, Cr₂O₃, MnO, and Mn₂O₃ oxides, rather than the oxides of Fe.

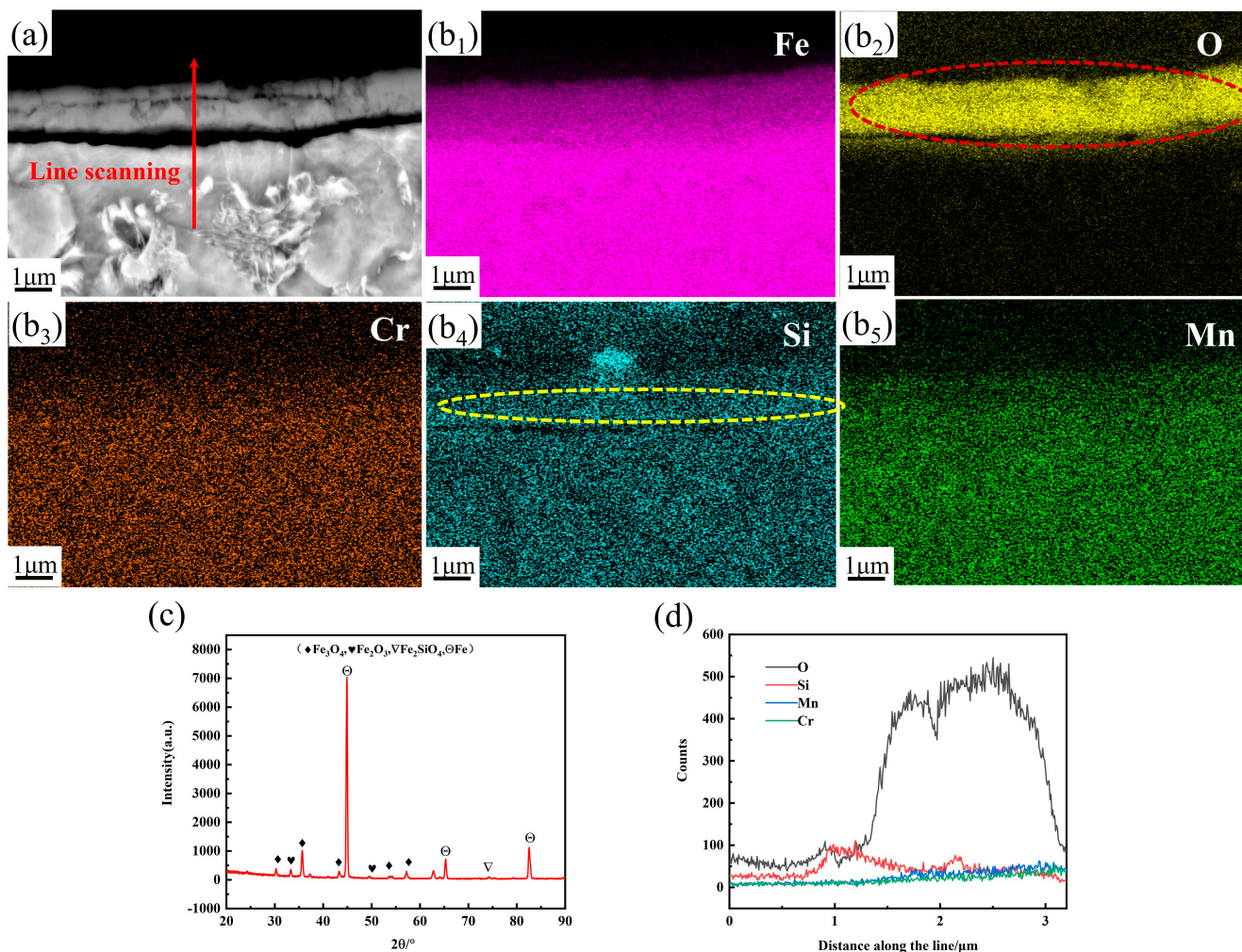


Figure 2. Longitudinal section SEM images of 22MnB5 studied steel soaked at 900 °C for 5 min. (a) The longitudinal section morphology; (b₁–b₅) EDS mapping of oxide layer; (c) XRD pattern of oxide layer; (d) EDS line scanning of (a) red arrow. The red circle is O enrichment, while the yellow circle is Si enrichment.

Taking into account the physical and chemical properties of Si, during the oxidation reaction, the Si element reacted with dissolved O on the metal surface; the dissolved O was diffused to the steel surface and precipitated to form SiO₂. As the oxidation process advanced inside the metal, the internal oxide met FeO to form Fe₂SiO₄ compounds, which were low solubility in FeO, and accumulated on the oxide layer rather than the metal surface. The Fe vacancy diffused through the Fe₂SiO₄ compound, and the Fe vacancy was diffused faster in the oxide scale than in the Fe₂SiO₄ compound. As the oxide scale continued to grow, the alloying elements in the matrix would not move with the migration of iron atoms. As for 38Cr3MnNbVMo steel with high Si content in the matrix, once the oxidation process continued to advance inside the steel matrix, these vacancies were trapped in the oxide layer. With the extension of oxidation time, Si elements were enriched and consumed at the interface between the oxide layer and the matrix. The oxidation products of Si gradually left the matrix/oxide interface. The Si concentration at the interface was reduced and the degree of enrichment at the interface was gradually weakened.

It is worth mentioning that Mn segregation appears in the SEM-EDS and EPMA mapping and line scanning results, but it is not detected in the XRD results. Therefore, the ultra-thin oxide layer with Fe₃O₄ is the main oxide layer structure, followed by spinel FeCr₂O₄, olivine Fe₂SiO₄, and Mn oxides.

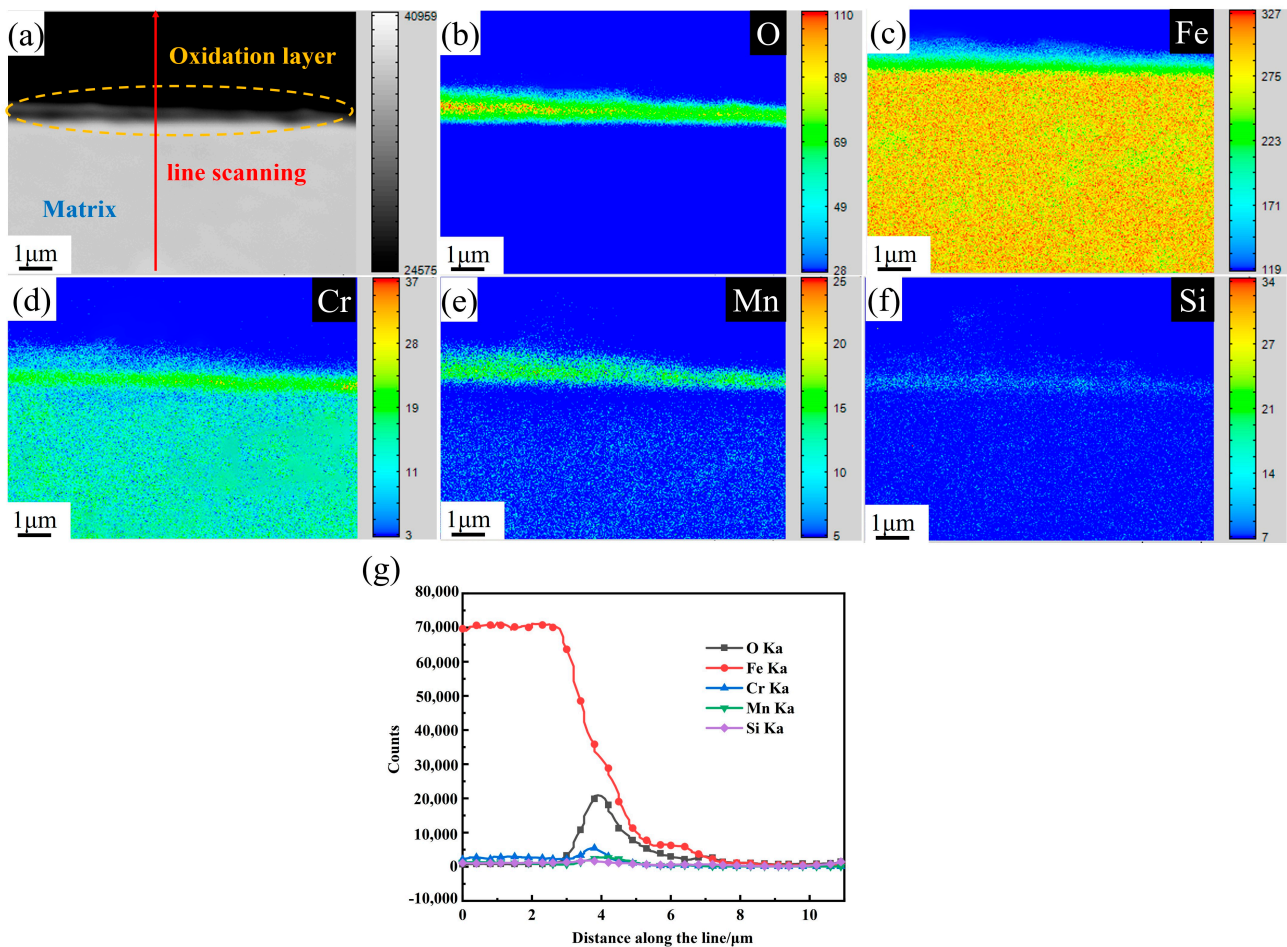


Figure 3. Longitudinal section EPMA images of 38Cr3MnNbVMo studied steel soaked at 900 °C for 5 min. (a) Longitudinal section EPMA images; (b–f) EPMA mapping distribution results of different elements; (g) EDS line scanning of (a) red arrow.

TEM characterization of the 38Cr3MnNbVMo ultra-thin oxide layer was performed, and TEM images are illustrated in Figure 4. Figure 4a is the morphology of the oxide layer, and the diffraction patterns show that the main structure of the oxide layer is Fe_3O_4 . According to Figure 4b,d and Table 2, it proves that the content of Cr, Si, and Mn at different locations is different, so the enrichment degree is different. These results are consistent with the results of SEM-EDS and EPMA. According to Figure 4c, the secondary oxide layer is closest to the base alloy; the purple dotted line in Figure 4a shows very fine grains and is mainly composed of Fe-Si olivine. However, the secondary oxide layer near the substrate is composed of Fe-Cr spinel, and their widths are clearly measured by TEM-EDS mapping analysis as 22 nm and 50 nm, respectively. Thus, it can be presumed that FeCr_2O_4 spinel is coated with Fe_2SiO_4 olivine. The inter-planar crystal spacing of the two enriched products is calculated by high-resolution IFFT as 0.3156 nm and 0.5431 nm, respectively.

The ultra-thin oxide layer of 38Cr3MnNbVMo hot-rolled tested steel is characterized by TEM and the sample preparation method is FIB micro-zone cutting technology. The TEM image of the ultra-thin oxide layer is shown in Figure 4. Figure 4a is the TEM topography of the oxide layer. Selected electron diffraction demonstrates that there is a Fe_3O_4 phase in the oxide layer. Due to the lower thickness of the oxide layer cut by FIB, the Fe_2O_3 phase in the outermost part of the oxide layer is not observed.

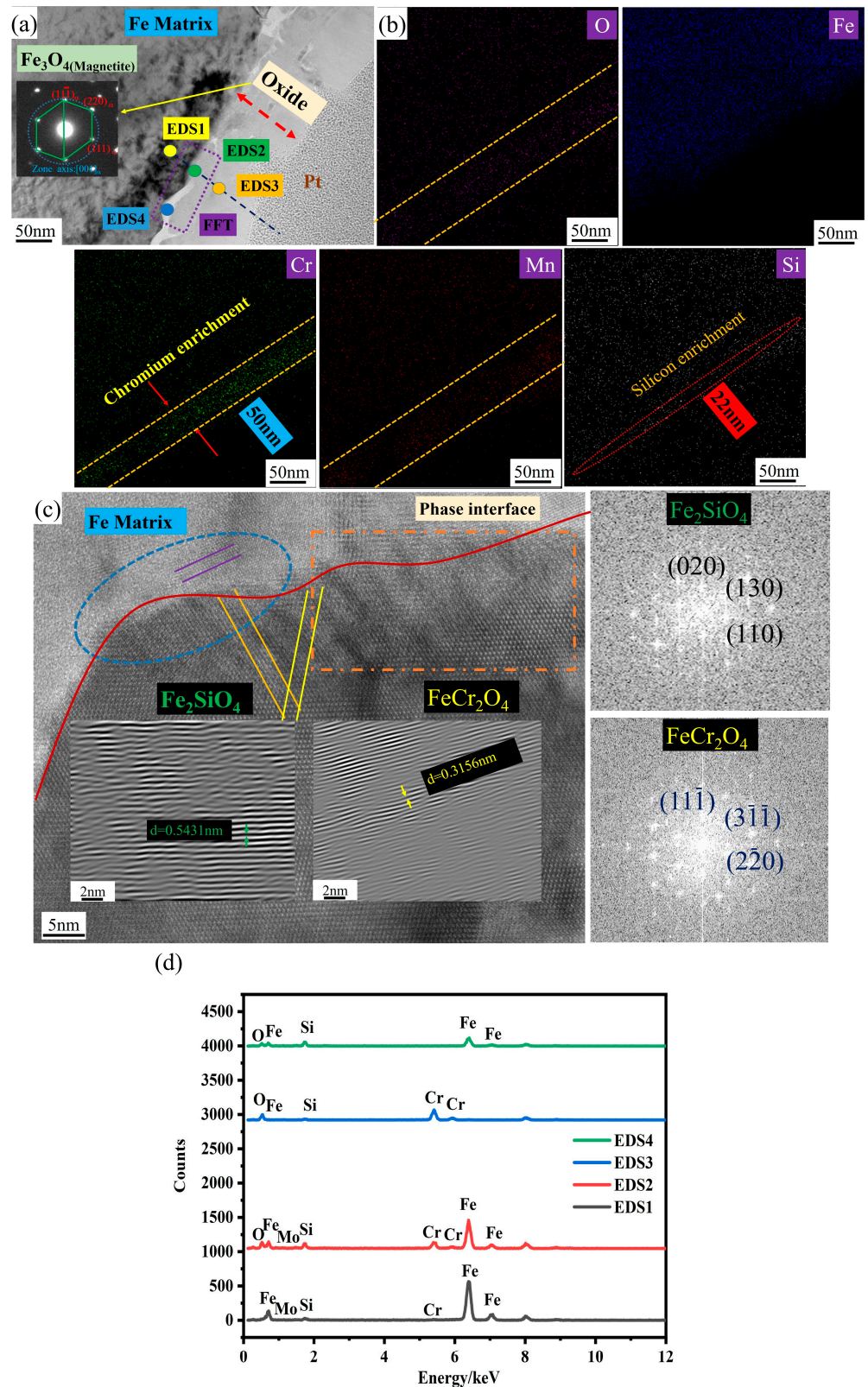


Figure 4. TEM characterization of ultra-thin oxide layer in 38Cr3MnNbVMo studied steel. (a) TEM morphology of oxide layer; (b) TEM-EDS mapping of oxide layer; (c) high-resolution TEM analysis of the interface between matrix and oxide layer; (d) TEM-EDS analysis at different locations in (a).

Combined with Figure 4b,d, it can be seen that the alloy oxide containing Si is closest to the matrix interface, which is consistent with the results characterized by SEM-EDS and

EPMA. High-resolution transmission analysis was performed on the part of the purple dashed line in Figure 4a. Figure 4c portrays the high-resolution transmission image, FFT and IFFT image of the alloy closest to the matrix at the interface between the matrix and the oxide layer. The oxide has very fine grain and is mainly composed of the Fe-Cr spinel oxide layer, while the closest to the matrix is the Fe-Si olivine oxide layer. Through the surface distribution diagram, we can clearly measure that the approximate widths of the two are 50 nm and 22 nm; it can be seen that FeCr_2O_4 has spinel-coated Fe_2SiO_4 olivine. By high-resolution IFFT calculation, the crystal face spacing of the two enriched products is 0.3156 nm and 0.5431 nm, respectively.

The formation mechanism concerning the ultra-thin oxide layer was discussed; specifically, the ultra-thin oxide layer of 38Cr3MnNbVMo hot-rolled steel after holding at 900 °C for 5 min under the condition of low oxygen partial pressure. First of all, the Si content of the 38Cr3MnNbVMo steel was high and the low-oxygen environment was mixed with argon and air, which affected the oxidation behavior of the Si element. On the influence of the low-oxygen environment on the alloy surface, the oxide of Si was assumed as the surface alloy coating, thus limiting the entry of O ions into the surface of the steel plate, and Si elements are more easily oxidized in the gas environment with low-oxygen content [19–23]. Onishi et al. [24] proved that the diffusion rate of Si was higher than O, and was forming a very thin SiO_2 layer on the alloy surface under the condition of low oxygen partial pressure. Internal oxidation occurred over a limited oxygen partial pressure range and was limited to alloys with Si concentrations below 1 wt.%. With the increment of Si content, the oxygen partial pressure of internal Si oxidation was decreased and external Si oxidation occurred.

Li et al. [25] believed that the increase in Si content enhanced the effective mutual diffusion coefficient, promoting the formation of Cr-containing oxides. Due to the small prior austenite grain size of 38Cr3MnNbVMo steel, Cr diffused rapidly to the substrate surface through the prior austenite grain boundary in the initial oxidation stage. According to the element diffusion mechanism, the dissolved O traversed the alloy oxide and reacted with the dissolved Cr diffused from the matrix side so as to form Cr_2O_3 oxide. As an active-reactive element, the Mn element reduced the critical Cr content in the continuous formation of Cr_2O_3 , while SiO_2 particles formed in the early stage and provided the formation of a continuous Cr_2O_3 layer nucleation site. The formation of Mn-rich oxides promoted the densification of the oxide layer and inhibited the internal diffusion of the O element. Therefore, it resulted in the reduction in oxygen partial pressure. The two synergistic effects promoted the outward oxidation of Cr and further formed the oxides Cr_2O_3 [26–28].

As the tested steel underwent oxidation from a high temperature to the cooling process, FeO was formed due to the reaction of Fe and O. When the Cr element replaced the Fe element in the oxide in the steel, the FeCr_2O_4 phase was formed. At the same time, the Si element acted similarly with the Cr element and formed SiO_2 , continuing to combine with the Fe ion to form Fe_2SiO_4 . The diffusion rate of Fe ions in Fe_2SiO_4 and FeCr_2O_4 was faster than Cr and Si ions. Therefore, it continued to enrich at the outer layer of oxidation while the Fe ions near the interface were depleted. After the initial transformation process of oxidation, a steady concentration gradient was established in the oxide sample. The Fe ions diffused from the matrix to pass through the alloy oxide and form Fe_3O_4 at the FeO interface. Due to the obstruction of the alloy oxide layer, the diffusion ability of Fe^{2+} and the diffusion ability of O ions and Fe ions was weakened at the interface of Fe_3O_4 , which can only stably form Fe_3O_4 and maintain the growth of the Fe_3O_4 layer.

Mn enrichment was observed during EPMA and TEM characterization, so the Mn oxide was enriched in the outer oxide layer. Thus, the ultra-thin oxide layer consisted of Fe_3O_4 , oxide of Mn, FeCr_2O_4 , Cr_2O_3 , and the Fe_2SiO_4 “healing layer”. In addition, the Mo element promoted the growth of Cr, Si, and Mn-rich oxide layers by hindering the internal diffusion of the O ion and the external diffusion of the Fe ion. Therefore, the Mo element improved the oxidation resistance of the tested steel; the higher the Mo content, the more prominent the synergistic protection mechanism was. [29,30].

4. Conclusions

In this study, we investigated a novel hot-stamped steel with a Cr-Mn-Si alloy system, which demonstrated superior high-temperature oxidation resistance compared with the traditional 22MnB5 hot-stamped steel. The main conclusions are as follows:

- (1) In 38Cr3MnNbVMo hot-stamped steel, under the condition of low oxygen partial pressure in argon and high Cr content, an ultra-thin oxide layer of 0.6 μm was formed after being held at 900 °C for 5 min. An enrichment region of Cr, Mn, and Si is formed near the matrix, which indicates that the oxides of Cr/Si/Mn hinder the diffusion of Fe ions in the matrix.
- (2) 38Cr3MnNbVMo hot-stamped steel shows the unique microstructure and element distribution characteristics of the Cr-Si-Mn oxide layer. Cr and Si are used as the core elements of the oxidation resistance of ultra-high-strength steel. The ultra-thin oxide layer is composed of Fe_3O_4 , Mn oxide, FeCr_2O_4 , Cr_2O_3 , and Fe_2SiO_4 . The Si element is easier to oxidize, and an ultra-thin Fe_2SiO_4 alloy oxide layer is formed at the matrix interface. It collaborates with the oxides of Cr and Mn to hinder the inward diffusion of external O ions and the outward diffusion of matrix Fe ions.
- (3) In a novel hot-stamped steel, the addition of the Mo element improves the antioxidant capacity, and a variety of antioxidant elements and alloy oxidation products effectively hinder the continuous growth of the oxide sheet. Ultimately, they improve the high-temperature antioxidant property of novel hot-stamped steel.

Author Contributions: Conceptualization, Y.Z. and L.L.; methodology, L.L.; software, W.L.; validation, Y.Z. and J.Y.; form analysis; D.Y. and W.L.; investigation, W.L. and D.Y.; resources, Z.Z. and J.Y.; data curation, Z.Z., Y.Z. and J.Y.; writing—original draft preparation, Y.Z. and L.L.; writing—review and editing, Y.Z., Z.Z. and J.Y.; visualization, J.Y.; supervision, Z.Z.; project administration, Z.Z. and J.Y.; funding acquisition, Z.Z. All authors have read and agreed to the published version of the manuscript.

Funding: This work was supported financially by the National Natural Science Foundation of China (No. 52174353); Major Scientific and Technological Innovation Project of CITIC Group (Grant Number 2022zxkya06100); Development and Application Research of Ultra-high Strength Hot Stamped Steel Strip for Automobile (Grant Number 2022-1100-43-006249).

Data Availability Statement: The raw data supporting the conclusions of this article will be made available by the authors on request.

Conflicts of Interest: The authors declare that this study received funding from Development and Application Research of Ultra-high Strength Hot Stamped Steel for Automobile (Grant Number 2022-1100-43-006249). The funder had the following involvement with the study: Jianlin Yu (Validation, Resources, Data curation, writing—review and editing, Visualization, Project administration). Author Jianlin Yu was employed by the company Xinyu Iron and Steel Group Co., Ltd., Xinyu, China. The remaining authors declare that the research was conducted in the absence of any commercial or financial relationships that could be construed as a potential conflict of interest.

References

1. Nikravesh, M.; Naderi, M.; Akbari, G.H. Influence of hot plastic deformation and cooling rate on martensite and bainite start temperatures in 22MnB5 steel. *Mater. Sci. Eng. A* **2012**, *540*, 24–29. [[CrossRef](#)]
2. Karbasian, H.; Tekkaya, A.E. A review on hot stamping. *J. Mater. Process. Technol.* **2010**, *210*, 2103–2118. [[CrossRef](#)]
3. Li, S.S.; Luo, H.W. Medium-Mn steels for hot forming application in the automotive industry. *Int. J. Miner. Metall. Mater.* **2021**, *28*, 741–753. [[CrossRef](#)]
4. Mori, K.; Bariani, P.; Behrens, B.-A.; Brosius, A.; Bruschi, S.; Maeno, T.; Merklein, M.; Yanagimoto, J. Hot stamping of ultra-high strength steel parts. *Cirp Ann.* **2017**, *66*, 755–777. [[CrossRef](#)]
5. Ding, W.; Gong, Y.; Lu, Q.; Wang, J.; Wang, Z.; Li, W.; Jin, X. Improve bendability of a Cr-alloyed press-hardening steel through an in-line quenching and non-isothermal partitioning process. *J. Manuf. Process.* **2022**, *84*, 481–493. [[CrossRef](#)]
6. Yoo, J.; Kim, S.; Jo, M.C.; Kim, S.; Oh, J.; Kim, S.H.; Lee, S.; Sohn, S.S. Effects of Al-Si coating structures on bendability and resistance to hydrogen embrittlement in 1.5-GPa-grade hot-press-forming steel. *Acta Mater.* **2022**, *225*, 117561. [[CrossRef](#)]
7. Wang, Z.; Cao, Z.H.; Wang, J.F.; Huang, M.X. Improving the bending toughness of Al-Si coated press-hardened steel by tailoring coating thickness. *Scr. Mater.* **2021**, *192*, 19–25. [[CrossRef](#)]

8. Chai, Z.; Wang, L.; Wang, Z.; Lu, Q.; Hu, J.; Sun, W.; Wang, J.; Xu, W. Cr-enriched carbide induced stabilization of austenite to improve the ductility of 1.7 GPa press-hardened steel. *Scr. Mater.* **2023**, *224*, 115108. [[CrossRef](#)]
9. Zhang, L.; Yan, W.; Shi, Q.; Li, Y.; Shan, Y.; Yang, K. Silicon enhances high temperature oxidation resistance of SIMP steel at 700 °C. *Corros. Sci.* **2020**, *167*, 108519. [[CrossRef](#)]
10. Huang, C.Y.; Chen, Y.; Lin, C.S. High-temperature oxidation resistance of hot stamping steel with chromium coating electroplated in trivalent chromium bath. *Mater. Today Commun.* **2022**, *33*, 104663. [[CrossRef](#)]
11. Mehtani, H.K.; Khan, M.I.; Jaya, B.N.; Parida, S.; Prasad MJ, N.V.; Samajdar, I. The oxidation behavior of iron-chromium alloys: The defining role of substrate chemistry on kinetics, microstructure and mechanical properties of the oxide scale. *J. Alloys Compd.* **2021**, *871*, 159583. [[CrossRef](#)]
12. Jin, X.J.; Chen, S.H.; Rong, L.J. Effects of Mn on the mechanical properties and high temperature oxidation of 9Cr2WVTa steel. *J. Nucl. Mater.* **2017**, *494*, 103–113. [[CrossRef](#)]
13. Li, Z.; Wang, L.; Wang, Z.; Zhang, T.; Wang, J.; Xu, W. Oxidation mechanisms of a Cr-Si alloyed coating-free press-hardened steel under simulated press hardening conditions. *Mater. Charact.* **2023**, *206*, 113446. [[CrossRef](#)]
14. Hou, Z.; Min, J.; Wang, J.; Lu, Q.; He, Z.; Chai, Z.; Xu, W. Effect of rapid heating on microstructure and tensile properties of a novel coating-free oxidation-resistant press-hardening steel. *JOM* **2021**, *73*, 3195–3203. [[CrossRef](#)]
15. Zhao, Y.; Yang, D.; Qin, Z.; Chu, X.; Liu, J.; Zhao, Z. A novel hot stamping steel with superior mechanical properties and antioxidant properties. *J. Mater. Res. Technol.* **2022**, *21*, 1944–1959. [[CrossRef](#)]
16. Zhao, Y.; Yang, D.; Zhou, F.; Liu, L.; Wang, P.; Gao, P.; Zhao, Z. Enhanced Strength and Ductility of 2.4 GPa Hot-Stamped Steel with an Extremely Thin Oxide Layer. *Steel Res. Int.* **2023**, *94*, 2200917. [[CrossRef](#)]
17. Cai, X.C.; Ding, S.J.; Jin, S.B.; Xu, L.D.; Liu, G.Y.; Sun, B.R.; Shen, T.D. Superior high-temperature oxidation resistance of nanocrystalline 304 austenitic stainless steel containing a small amount of Si. *Scr. Mater.* **2021**, *204*, 114155. [[CrossRef](#)]
18. Genève, D.; Rouxel, D.; Pigeat, P.; Weber, B.; Confente, M. Surface composition modification of high-carbon low-alloy steels oxidized at high temperature in air. *Appl. Surf. Sci.* **2008**, *254*, 5348–5358. [[CrossRef](#)]
19. Buscail, H.; Issartel, C.; Riffard, F.; Rolland, R.; Perrier, S.; Fleurentin, A. Influence of various gaseous environments on SiO₂ formation on the 330Cb (Fe-35Ni-18Cr-1Nb-2.15Si) alloy at 900 °C. *Corros. Sci.* **2012**, *65*, 535–541. [[CrossRef](#)]
20. Dong, H.; Wang, P.; Li, D.; Li, Y. Effect of pre-deformation on the oxidation resistance of a high Si ferritic/martensitic steel in oxygen-saturated stagnant lead-bismuth eutectic at 550 °C. *Corros. Sci.* **2017**, *118*, 129–142. [[CrossRef](#)]
21. Buscail, H.; Issartel, C.; Riffard, F.; Rolland, R.; Perrier, S.; Fleurentin, A.; Josse, C. Effect of various lanthanum sol-gel coatings on the 330Cb (Fe-35Ni-18Cr-1Nb-2Si) oxidation at 900 °C. *Appl. Surf. Sci.* **2011**, *258*, 678–686. [[CrossRef](#)]
22. Mori, K.; Ito, D. Prevention of oxidation in hot stamping of quenchant steel sheet by oxidation preventive oil. *CIRP Ann.* **2009**, *58*, 267–270. [[CrossRef](#)]
23. Jacob, Y.; Haanappel, V.; Stroosnijder, M.; Buscail, H.; Fielitz, P.; Borchardt, G. The effect of gas composition on the isothermal oxidation behaviour of PM chromium. *Corros. Sci.* **2002**, *44*, 2027–2039. [[CrossRef](#)]
24. Onishi, T.; Nakakubo, S.; Takeda, M. Calculations of internal oxidation rate equations and boundary conditions between internal and external oxidation in silicon containing steels. *Mater. Trans.* **2010**, *51*, 482–487. [[CrossRef](#)]
25. Li, B.; Gleeson, B. Effects of silicon on the oxidation behavior of Ni-base chromia-forming alloys. *Oxid. Met.* **2006**, *65*, 101–122. [[CrossRef](#)]
26. Yun, D.W.; Seo, S.M.; Jeong, H.W.; Yoo, Y.S. The effects of the minor alloying elements Al, Si and Mn on the cyclic oxidation of Ni-Cr-W-Mo alloys. *Corros. Sci.* **2014**, *83*, 176–188. [[CrossRef](#)]
27. Suzuki, Y.; Yamashita, T.; Sugimoto, Y.; Fujita, S.; Yamaguchi, S. Thermodynamic analysis of selective oxidation behavior of Si and Mn-added steel during recrystallization annealing. *ISIJ Int.* **2009**, *49*, 564–573. [[CrossRef](#)]
28. Chai, Z.; Lu, Q.; Tedesco, S.; Shi, M.; Coryell, J.; Reini, L.; Lai, Q.; Wang, J.; Wang, L.; Xu, W. Investigation on mechanical properties and oxidation behavior of 1.2 and 1.7 GPa grades coating-free press-hardened steels. *Metals* **2023**, *13*, 489. [[CrossRef](#)]
29. Zhang, C.; Zhang, Y.; Hu, J.; Wang, Z.; Xue, J.; Yu, H.; Zhang, C.; Wang, X.; Cai, Q.; Wang, C.; et al. Effect of Mo on the high-temperature oxidation behavior of Cr-Ni-Mo hot-work die steels. *Corros. Sci.* **2023**, *224*, 111487. [[CrossRef](#)]
30. Zheng, Z.; Wang, S.; Long, J.; Wang, J.; Zheng, K. Effect of rare earth elements on high temperature oxidation behaviour of austenitic steel. *Corros. Sci.* **2020**, *164*, 108359. [[CrossRef](#)]

Disclaimer/Publisher’s Note: The statements, opinions and data contained in all publications are solely those of the individual author(s) and contributor(s) and not of MDPI and/or the editor(s). MDPI and/or the editor(s) disclaim responsibility for any injury to people or property resulting from any ideas, methods, instructions or products referred to in the content.